

AN EXPERIMENTAL STUDY OF ${}^9\text{Be}+{}^9\text{Be}$ REACTIONS BETWEEN LAB ENERGIES OF 3 AND 16 MeV

RICHARD C. YORK and R. T. CARPENTER

Department of Physics and Astronomy, The University of Iowa, Iowa City, Iowa 52242

Received 19 July 1976

(Revised 23 December 1976)

Abstract: Absolute cross sections were measured for elastic scattering of ${}^9\text{Be}$ on ${}^9\text{Be}$ at lab energies of 5, 9, 12 and 16 MeV. These differential cross sections were fit with a computer code to ascertain optical model parameters. Absolute differential cross sections were measured at lab energies of 5 and 12 MeV for the reactions ${}^9\text{Be}[{}^9\text{Be}, (p, t, \alpha)]{}^{17}\text{N}, {}^{15}\text{N}, {}^{14}\text{C}$.

E NUCLEAR REACTIONS ${}^9\text{Be}({}^9\text{Be}, {}^9\text{Be}), ({}^9\text{Be}, p), ({}^9\text{Be}, t), ({}^9\text{Be}, \alpha), E = 5, 9, 12, 16$ MeV; measured $\sigma(E, \theta)$, deduced optical model parameters. Natural target.

1. Introduction

This work consists of the first experimental investigation of the interaction of energetic beams of ${}^9\text{Be}$ with ${}^9\text{Be}$. Because of the low neutron binding energy of ${}^9\text{Be}$ and the diffuseness of its surface, it might be expected that this reaction would show some unusual features.

The elastic scattering data is discussed in sect. 2. The data are well described by an optical model fit and reasonable optical model parameters are extracted. The reactions which yield protons, tritons, and α -particles are discussed in sect. 3. At the low bombarding energies available, the cross sections for the production of all states which could be resolved are quite low, from 1 to 200 $\mu\text{b}/\text{sr}$. The angular distributions are for the most part featureless. It would therefore seem that a direct reaction interpretation is doubtful.

2. ${}^9\text{Be}$ on ${}^9\text{Be}$ elastic scattering

2.1. EXPERIMENTAL PROCEDURE

The ion source used to produce the beryllium beams has been previously described¹⁾. Essentially it is a standard High Voltage Engineering Corporation ion source with the entrance canal and sleeve replaced by specially made units of beryllium metal and beryllium oxide, respectively, with additional beryllium dust scattered inside the bottle so as to adhere to the walls and with chlorine as the gas. When hydrogen or helium is used as the gas, beams of these ions are obtained as usual. The University of Iowa type CN Van de Graaff is equipped with a deflection magnet in the terminal which serves as a mass analyzer after the ions have been accelerated by 10 to 20 keV.

The beryllium ions are separated from other ions extracted from the source and no contaminant beams are accelerated down the tube.

Carbon stripping foils may be inserted at a distance of five-twelfths of the way down the tube so that energies greater than 6 MeV maximum terminal voltage may be obtained. Stripped ${}^9\text{Be}$ beams allowed theoretical maximum lab energies of 16.5 MeV (${}^9\text{Be}^{+4}$), 13 MeV (${}^9\text{Be}^{+3}$), and 9.5 MeV (${}^9\text{Be}^{+2}$) assuming a maximum terminal energy of 6 MeV. (A typical carbon foil lasted from 1 to 5 h when used to strip beryllium beams.) Routinely observed current values for energy analyzed ${}^9\text{Be}$ beams were 20 to 200 nA for ${}^9\text{Be}^{+1}$, ${}^9\text{Be}^{+2}$ and ${}^9\text{Be}^{+3}$, and 1 to 20 nA for ${}^9\text{Be}^{+4}$ where ion charge dependence has not been considered in beam current values.

Self-supporting beryllium targets were made by vacuum evaporation of beryllium onto soap-covered glass slides from a tantalum boat using standard thin film techniques. Gold was evaporated in the same step in amounts such that the counting rates for ${}^9\text{Be}({}^9\text{Be}, {}^9\text{Be}){}^9\text{Be}$ and ${}^{197}\text{Au}({}^9\text{Be}, {}^9\text{Be}){}^{197}\text{Au}$ were the same order of magnitude. The targets were from 20 to 100 $\mu\text{g}/\text{cm}^2$ thick and had major contaminants of ${}^{12}\text{C}$, ${}^{16}\text{O}$, and a heavier element thought to be tantalum.

A ΔE - E telescope was used to detect the scattered ${}^9\text{Be}$ beam. The ΔE detector was a gas proportional counter designed by Von Behren²). The proportional counter had a FORMVAR entrance window about 200 keV thick to 5 MeV ${}^9\text{Be}$ and used a gas mixture of 95 % argon and 5 % CO_2 at pressures of 2 to 5 Torr. The E -detector, mounted behind the active proportional counter region in the gas itself, was a surface barrier solid state detector 150 μm in thickness. The telescope subtended an angular range of $\approx 1^\circ$.

The ΔE and E detector signals were amplified separately and fed into ADC units interfaced to an on-line computer. A CDC 160-A was used as an on-line computer in which a $\Delta E \times E$ (64×256) matrix was developed as data came in. The computer was interfaced to an oscilloscope such that the two-dimensional $\Delta E \times E$ matrix could be displayed at various contour levels. The events resulting from detection of ${}^9\text{Be}$ particles were marked on the contour by two lines. All events falling between these two lines were recorded as a single 1024 channel pulse height spectrum. It was this spectrum which was used to determine the elastic cross sections. These data were transferred to magnetic tape at the completion of each angle, the computer memory erased, and a new angle begun.

The $\Delta E \times E$ data demonstrated the necessity of utilizing a telescope for particle identification. Although not explicitly analyzed, energy loss lines resulting from alphas, lithium, and heavier elements, thought to be carbon and boron, were seen.

The limited angular range of the distributions was the result of interference of target contaminants (${}^{12}\text{C}$, ${}^{16}\text{O}$) at forward angles and the difficulty of separating the low-energy part of the ${}^9\text{Be}$ energy loss line from the heavier element energy loss lines in the $\Delta E \times E$ matrix at the backward angles.

2.2. DATA ANALYSIS AND RESULTS

The events from ${}^{197}\text{Au}({}^9\text{Be}, {}^9\text{Be}){}^{197}\text{Au}$ were assumed to be due to classical Rutherford scattering at all angles and energies investigated. With this assumption, the data was reduced to yield the elastic cross section of ${}^9\text{Be}({}^9\text{Be}, {}^9\text{Be}){}^9\text{Be}$ in the form of the ratio of measured cross section to theoretical Mott cross section³⁾ using the Rutherford scattering as normalization.

TABLE 1

Elastic scattering cross sections for ${}^9\text{Be}$ on ${}^9\text{Be}$ expressed as the ratio of the measured cross section to the theoretical Mott cross section

c.m. angle (deg)	Lab beam energy (MeV)			
	5	9	12	16
40				0.338 ± 0.010
50				0.170 ± 0.026
60	0.907 ± 0.038	0.408 ± 0.012	0.228 ± 0.007	0.245 ± 0.014
65	0.905 ± 0.030	0.379 ± 0.014	0.255 ± 0.006	
70	0.898 ± 0.027	0.352 ± 0.012	0.277 ± 0.010	
75	0.891 ± 0.022	0.339 ± 0.016	0.264 ± 0.015	
80	0.872 ± 0.018	0.332 ± 0.007	0.246 ± 0.004	0.160 ± 0.013
85	0.880 ± 0.022	0.313 ± 0.009	0.190 ± 0.005	
90	0.853 ± 0.034	0.312 ± 0.011	0.191 ± 0.007	0.142 ± 0.016
95	0.837 ± 0.055	0.309 ± 0.017	0.194 ± 0.010	
100	0.823 ± 0.065	0.332 ± 0.023	0.246 ± 0.016	0.180 ± 0.053
105	0.861 ± 0.067	0.340 ± 0.025	0.262 ± 0.019	
110	0.830 ± 0.060	0.352 ± 0.026	0.275 ± 0.020	
115	0.838 ± 0.054	0.379 ± 0.027	0.256 ± 0.019	
120	0.830 ± 0.053	0.404 ± 0.029	0.230 ± 0.017	

TABLE 2

Yield curve data at 45° lab angle for ${}^9\text{Be}$ on ${}^9\text{Be}$ expressed as in table 1

Lab beam energy (MeV)	Ratio to Mott at 45° lab	Lab beam energy (MeV)	Ratio to Mott at 45° lab
3.0	1.004 ± 0.056	5.0	0.853 ± 0.035
3.5	0.980 ± 0.048	5.25	0.796 ± 0.034
4.0	0.985 ± 0.053	9.0	0.312 ± 0.011
4.25	0.923 ± 0.053	12.0	0.191 ± 0.007
4.5	0.937 ± 0.053	16.0	0.142 ± 0.016
4.75	0.936 ± 0.042		

The final experimental results are given in tables 1 and 2. The errors given for the experimental points are relative and are due to error in summing the peaks, counting statistics, and the 1° angular range subtended by the telescope. The yield curve data used to normalize the ratios are given in table 2 and graphically displayed in fig. 1. Table 2 represents, at most energies, the average of results of several experiments with different targets. These different data gave cross-section ratios which were

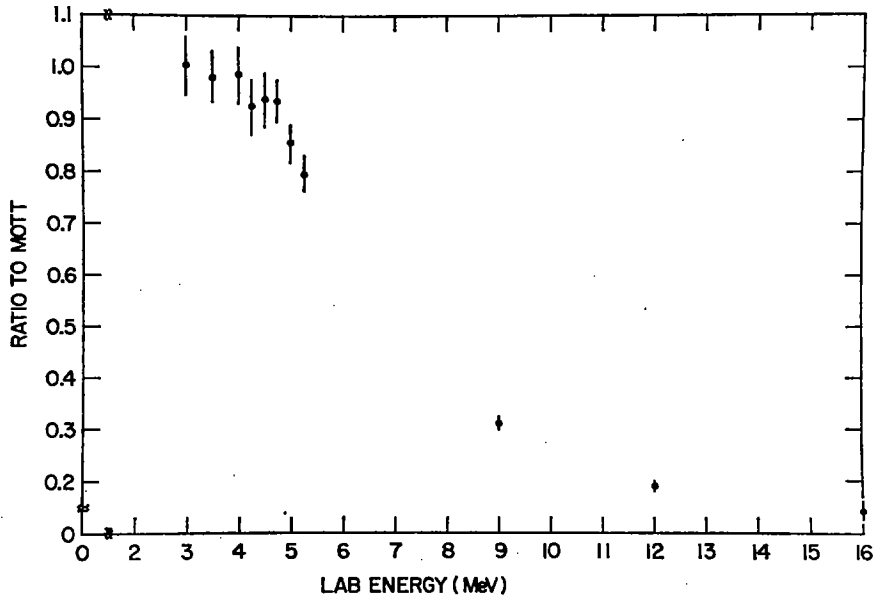


Fig. 1. Yield curve data at 45° lab angle for ${}^9\text{Be}$ on ${}^9\text{Be}$ expressed as the ratio of the measured cross section to the theoretical Mott cross section for lab energies 3 to 16 MeV.

consistent within $\pm 5\%$. On this basis, the absolute cross-section error is conservatively claimed to be $\leq \pm 10\%$.

The experimental data were fit with an optical model computer code which was a modified version of an elastic scattering search program written by Smith ⁴). The optical model code had six parameters available as variables. The real part of the nuclear potential was a Woods-Saxon potential with a well depth V , radius R , and diffuseness a_r . The imaginary part of the nuclear potential, which was either given by the derivative of the real potential form factor or by a Gaussian form factor, was described by a well depth W , a well radius R' and a diffuseness a_i .

The search procedure used was somewhat less extensive, but otherwise similar to that described in detail by Poling *et al.* ⁵). To summarize, it was found that no better data fits were given when six parameters were allowed than when only four parameters were used and that either form of the imaginary potential yielded equally good fits, though actual parameter values differed somewhat. On this basis all optical model data listed in table 3 used a derivative form factor and were limited to four parameters by demanding $R = R'$ and $a_r = a_i = a$. The well known ambiguity involving the constancy of the product VR^n , which is extensively explored by Poling *et al.* ⁵) for lithium elastic scattering, was found to exist for the present data with n on the order of 1.5 to 2.0. Different values of the product VR^n correspond to different numbers of wavelengths contained in the well. For the fits discussed below the potential radii were held constant and a family of potential well depths found.

TABLE 3

Sets of optical model parameters which gave good fits to the ^9Be on ^9Be elastic scattering data

Set	Beam energy lab (MeV)	$a_r = a_1$ ^{a)} (fm)	V ^{b)} (MeV)	W ^{c)} (MeV)	χ^2 ^{d)}
A-1	5	0.622	187.2	2.8	5.15
	9			18.6	0.825
	12			30.5	1.06
	16 ^{e)}			42.3	3.01
C-1	5 ^{f)}	0.632	189.3	6.6	2.58
	9 ^{f)}			22.2	0.325
	12 ^{f)}			33.9	1.15
	16 ^{f)}			49.6	4.34
C-2	5	0.621	228.4	7.7	2.57
	9			24.8	0.32
	12			37.6	1.09
	16			54.6	4.61
C-3	5	0.610	271.3	8.6	2.61
	9			27.1	0.315
	12			41.1	1.05
	16			59.6	4.87
C-4	5	0.601	318.2	9.2	2.67
	9			29.3	0.312
	12			44.4	1.02
	16			64.5	5.11
C-5	5	0.592	369.0	9.6	2.78
	9			31.3	0.309
	12			47.6	0.992
	16			69.3	5.36
A-6	5 ^{e)}	0.599	423.7	17.7	1.87
	9			42.5	0.839
	12			61.1	1.10
	16			86.0	6.42
C-6	5	0.584	423.7	9.7	2.91
	9			33.1	0.306
	12			50.6	0.976
	16			73.9	5.60
B-7	5	0.565	485.1	8.2	3.28
	9			29.8	0.986
	12 ^{e)}			46.1	0.848
	16			67.7	4.63
C-7	5	0.577	482.1	9.6	3.08
	9 ^{e)}			34.7	0.304
	12			53.5	0.972
	16			78.6	5.84

$R = R_A A^{1/3}$ is the Woods-Saxon potential radius; $R' = R_B A_T^{1/3}$ is the imaginary potential radius; A_T = target mass. The radii $R_A = R_B = 2$ fm for all values in the table.

^{a)} a_r = Woods-Saxon potential diffuseness; a_1 = imaginary potential diffuseness.

^{b)} V = Woods-Saxon potential well depth.

^{c)} W = imaginary potential well depth.

^{d)} The χ^2 values as defined in Poling ⁵⁾ were not computed with the exact weighting factors for each point (3.2% error for all points assumed), and therefore are only valid for fit comparison.

^{e)} Optical model parameter set giving lowest χ^2 value for a given energy (graphed for 5 and 16 MeV as broken curve).

^{f)} Optical model parameter set used to produce smooth curves in figs. 3 through 6 (lowest χ^2 sum value).

The results of the optical model fits are given in table 3. The data in table 3 were generated in the following manner. The A-sets represent the best fit to the 12 MeV data obtained by searching on V , W and a . The 9 MeV parameters in the A-data sets were obtained by fixing a and V to be equal to that obtained for 12 MeV A-set values and searching only on W . The B-sets represent the best fit to the 9 MeV data when searching on W and V while keeping the a -value equal to the value found in set A. The 12 MeV parameters in the B-data sets were obtained by fixing a and V to be equal to the 9 MeV B-set parameters and searching on W only. The C-data sets represent the best fit to the 9 MeV data obtained by searching on V , W and a . The 12 MeV parameters in the C-sets were obtained by fixing a and V equal to the 9 MeV C-set values and searching on W only. Set C invariably yielded the lowest overall value of chi-square.

Parameter searches were not done on the 16 MeV data because there were too few experimental points to merit doing so. Therefore the 16 MeV optical model parameters listed in table 3 were the result of keeping a , R and V constant within a set, and assuming W varies linearly with energy. Parameter W was calculated using the 9 and 12 MeV parameters.

Searches were done on the 5 MeV data. However, the fits proved unstable, yielding values for W an order of magnitude greater than those for 12 MeV at best, and at worst negative values for W . The 5 MeV optical model parameters in table 3 then were, as before, the result of keeping a , R and V constant within a set and assuming a linearly varying W , calculated using the 9 and 12 MeV parameters. A visual inspection of the 5 MeV data (see fig. 2) implies that the distribution shape is basically a straight line within error bars. Perhaps better fits could be obtained by searching on data smoothed to a straight line. Furthermore, the quoted $\pm 10\%$ absolute error would allow additional freedom in experimental data manipulation with an eye toward better fits.

It was found that all of the first eight or nine partial waves contributed significantly to the cross sections given by the optical model fits. This implies that the interior of the well is important and therefore the surface dependent "Igo ambiguity" is not expected to apply. Reasonable data fits were not possible for real well depths less than about 90 MeV and smaller well radii also yielded poorer fits. The rather standard diffuseness values obtained do not substantiate a picture of beryllium with an unusually diffuse surface, although attempts were made to force parameter sets into this regime.

The experimental angular distributions are displayed graphically in figs. 2 through 5. The data point error bars represent relative errors only. Set C-1 gave the best overall fit to the data, and it was this parameter set which was used in the optical model computer code to produce the smooth curves in figs. 2 through 5. Since only W was allowed to vary within a set, these smooth curves show the consistency of the optical model theory with that constraint. While set C-1 represents the best overall fit to the data, better fits were obtained for individual angular distributions. These

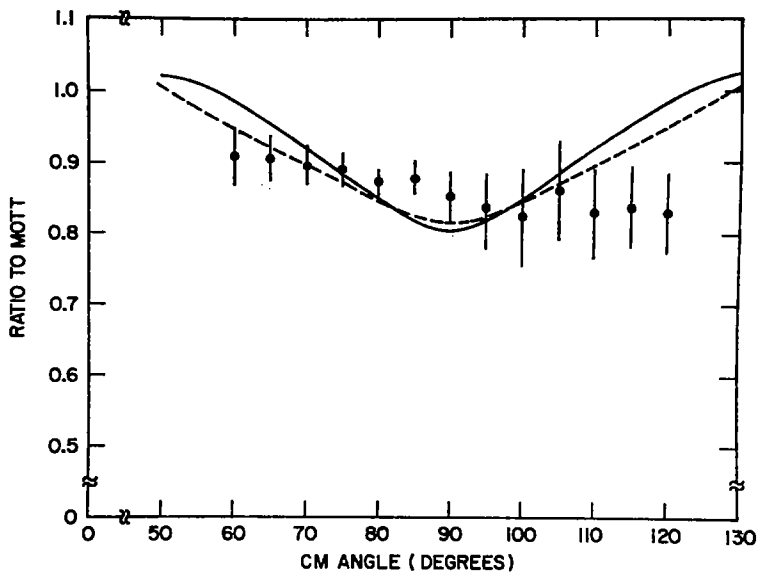


Fig. 2. Elastic scattering distribution for ${}^9\text{Be}$ on ${}^9\text{Be}$ at 5 MeV lab energy, expressed as in fig. 1.

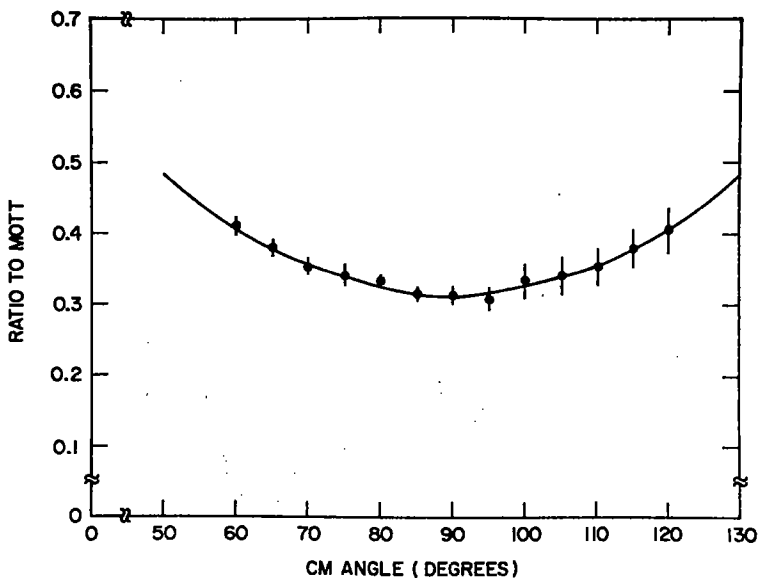


Fig. 3. Elastic scattering distribution for ${}^9\text{Be}$ on ${}^9\text{Be}$ at 9 MeV lab energy, expressed as in fig. 1.

best individual fits are shown as a broken curve in figs. 2 and 5 for the 5 and 16 MeV data, respectively.

Because of the limited energy range available it is not known what physical meaning, if any, these optical model parameter fits have. However, the 9 and 12 MeV

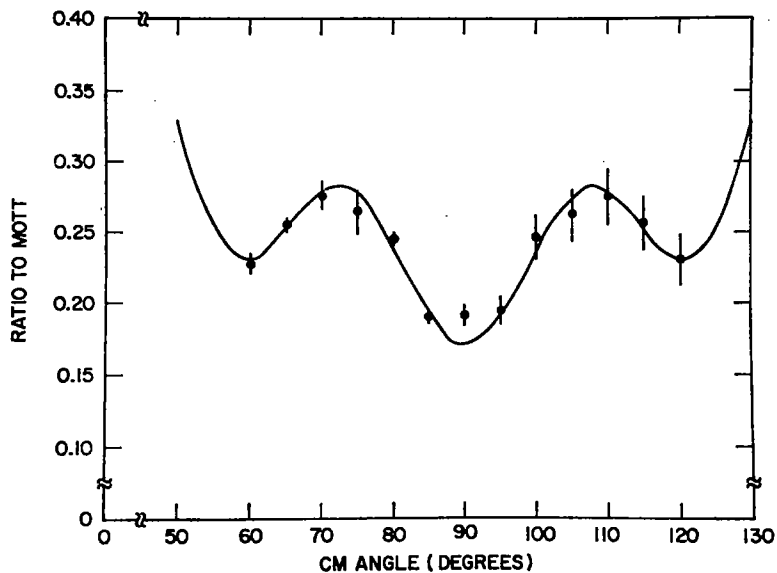


Fig. 4. Elastic scattering distribution for ${}^9\text{Be}$ on ${}^9\text{Be}$ at 12 MeV lab energy, expressed as in fig. 1.

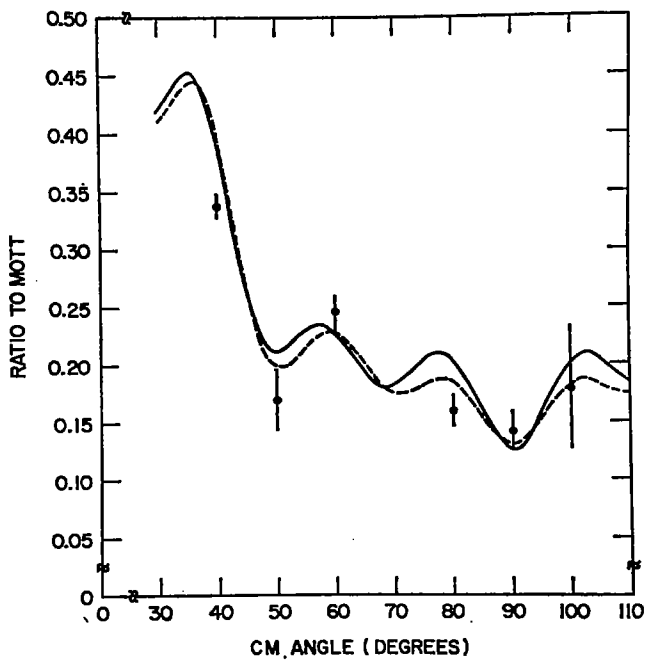


Fig. 5. Elastic scattering distribution for ${}^9\text{Be}$ on ${}^9\text{Be}$ at 16 MeV lab energy, expressed as in fig. 1.

optical model parameters differ only in W , and, as discussed above, the 5 MeV fits might be improved with fewer constraints. It is known ⁵⁾ that, in the case of the elastic scattering of lithium, optical model parameter sets obtained from the analysis of low energy data are better able to fit high energy elastic scattering data than high energy parameter sets can fit the low energy data. There is no reason to suspect the situation is otherwise in the case of beryllium scattering, but one must of course await the high energy data to be sure.

3. ${}^9\text{Be}$ on ${}^9\text{Be}$ reactions

3.1. EXPERIMENTAL PROCEDURE

The targets were made in exactly the same manner as described in the elastic scattering section. However, the targets used for the reaction data were somewhat thicker (50–200 $\mu\text{g}/\text{cm}^2$).

A trial experiment demonstrated the necessity of accumulating data at one angle for periods of ten to twenty hours to get good statistics ($\approx 10\%$). Because of this fact, a detector system which allowed data to be taken at three angles simultaneously was employed. Three ΔE - E telescopes were mounted on the moveable top plate of the scattering chamber. The three telescopes had a fixed angular separation of 30° with respect to each other, and the whole telescope system was moveable with respect to the beam. The ΔE detectors were surface barrier solid state detectors 40 μm thick. The E -detectors were surface barrier solid-state detectors 2000 μm in thickness. Each telescope subtended a solid angle of 1.09 msr.

A monitor detector was mounted on the opposite side of the chamber at 45° lab angle. This detector was also a surface barrier solid-state detector 150 μm thick. The pulse height spectrum for this detector was used to normalize the cross-section yields for a single angular setting of the telescope assembly. The monitor was a single detector, and therefore the resulting spectrum was that of all particle types. A program was written for the on-line computer which separated the events from ${}^9\text{Be}$ on ${}^9\text{Be}$ elastic scattering from other events and used to obtain the number of events from ${}^9\text{Be}({}^9\text{Be}, {}^9\text{Be}){}^9\text{Be}$. The reaction cross sections were normalized absolutely using the number of ${}^9\text{Be}$ on ${}^9\text{Be}$ elastic events given by the monitor spectrum and the measured elastic cross sections given in the previous section.

3.2. RESULTS

The absolute differential cross sections are shown graphically in figs. 9 through 11. The errors shown are relative only. These relative errors are the result of counting statistics in reaction peaks and error in obtaining the number of ${}^9\text{Be}$ on ${}^9\text{Be}$ elastic events from the monitor spectrum. The error in the number of ${}^9\text{Be}$ on ${}^9\text{Be}$ elastic events was, in general, the largest contributor ($\pm 20\%$) because of the necessity of separating these events from a background of reaction products. The stated $\pm 20\%$ error for this error is very conservative and may well be as little as 10% . The possible

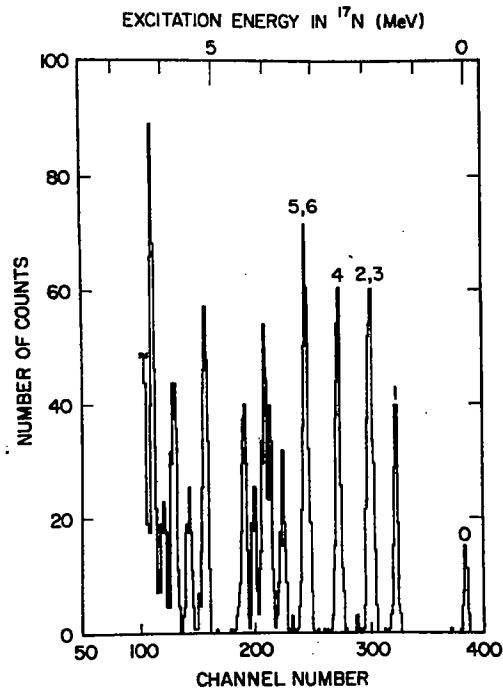


Fig. 6. Representative 1024 channel proton spectrum of ${}^9\text{Be}({}^9\text{Be}, p){}^{17}\text{N}$ at 30° and 5 MeV lab.

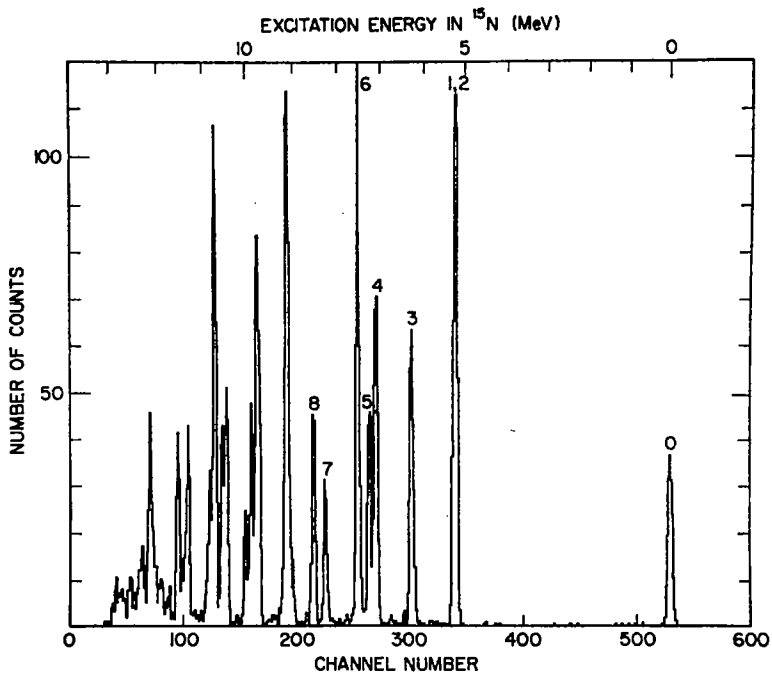


Fig. 7. Representative 1024 channel triton spectrum of ${}^9\text{Be}({}^9\text{Be}, t){}^{15}\text{N}$ at 30° and 12 MeV lab.

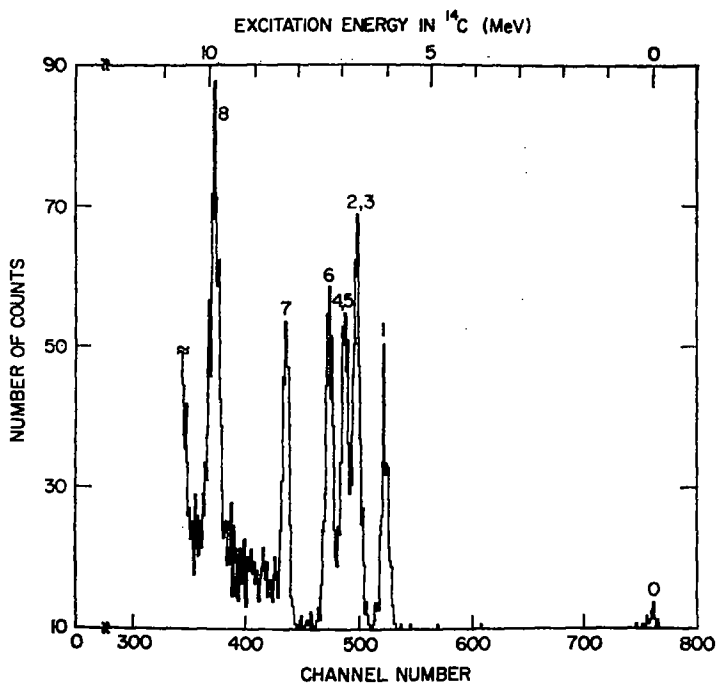


Fig. 8. Representative 1024 channel α -spectrum of $^9\text{Be}(^9\text{Be}, \alpha)^{14}\text{C}$ at 50° and 5 MeV lab.

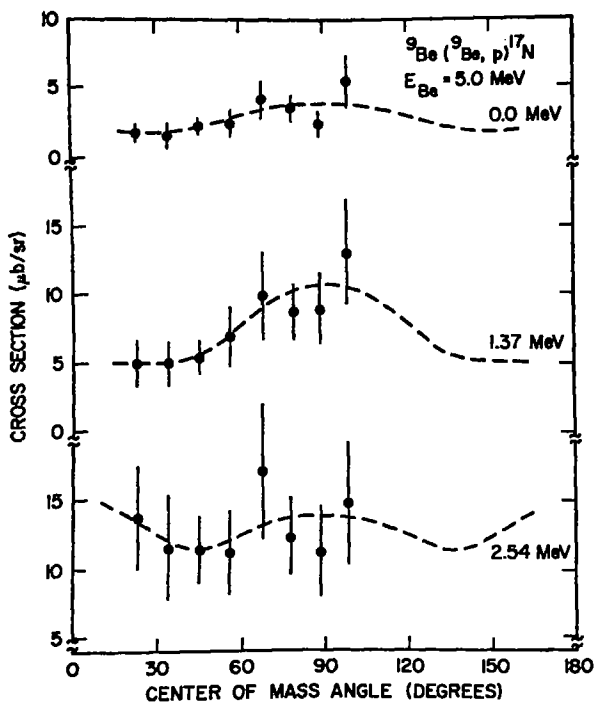


Fig. 9. Differential cross sections for $^9\text{Be}(^9\text{Be}, p)^{17}\text{N}$. The dashed curves are to guide the eye and indicate the required symmetry about 90° .

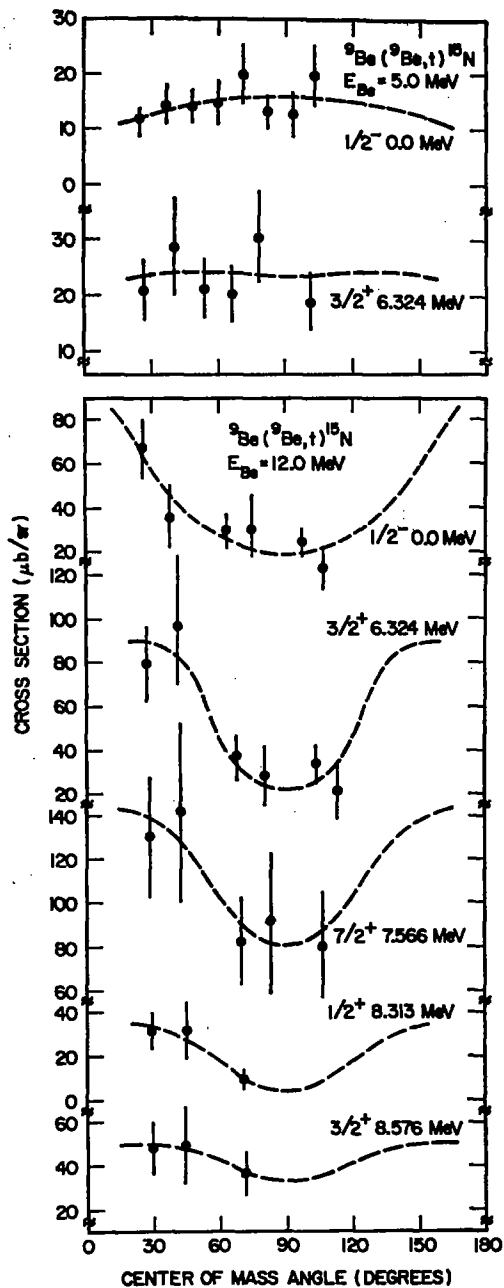


Fig. 10. Differential cross sections for ${}^9\text{Be}({}^9\text{Be}, t){}^{15}\text{N}$. See caption to fig 9.

$\pm 10\%$ normalization error in the absolute elastic cross sections has not been included in the errors given.

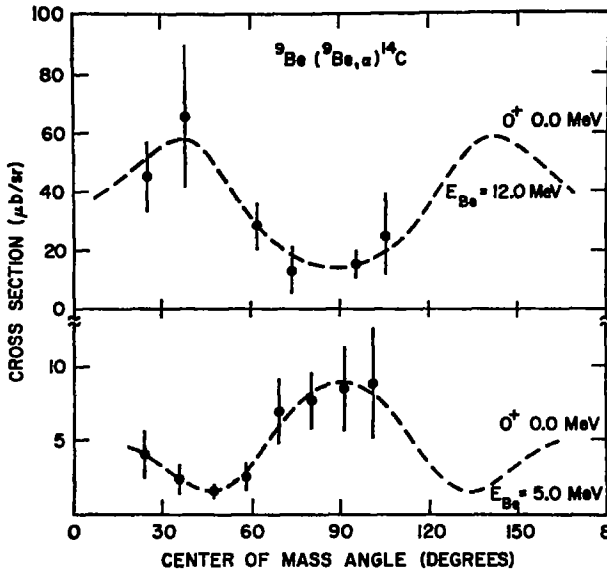


Fig. 11. Differential cross sections for ${}^9\text{Be}({}^9\text{Be}, \alpha){}^{14}\text{C}$. See caption to fig. 9.

Data analysis was limited to states resolvable over the angular range of data taken. For this reason the results of the ${}^9\text{Be}({}^9\text{Be}, d){}^{16}\text{N}$ were not analyzed.

A typical proton spectrum is shown in fig. 6. The numbers indicate the excited state in ${}^{17}\text{N}$. Angular distributions for the resolved states are shown in fig. 9. Proton data was analyzed only for 5 MeV lab energy. No data analysis of the 12 MeV proton spectrums was done because of very poor statistics and unresolved states. As can be seen the cross sections are extremely small (2–22 $\mu\text{b}/\text{sr}$) and have no structure. In general, the higher excited states have larger cross sections.

A representative triton spectrum is shown in fig. 7. The numbers indicate the excited state in ${}^{15}\text{N}$. Angular distribution for the resolved states are shown in fig. 10. The angular distributions have very little structure. The cross sections increased significantly both with bombarding energy and excited state number. Once again, these cross sections were very small, ranging from 8 to 40 $\mu\text{b}/\text{sr}$ at 5 MeV lab bombarding energy and from 4 to 180 $\mu\text{b}/\text{sr}$ at 12 MeV lab bombarding energy.

A typical α -spectrum is shown in fig. 8. The numbers indicate the excited state in ${}^{14}\text{C}$.

With respect to other reaction channels, little information is now available. The ${}^9\text{Be}({}^9\text{Be}, {}^8\text{Be}){}^{10}\text{Be}$ reaction was studied sufficiently to determine that there is no significant (less than 1 μb) contribution from this channel. Other reaction channel data, e.g., ${}^9\text{Be}({}^9\text{Be}, {}^{17}\text{O})\text{n}$ were not studied.

4. Conclusion

The ^9Be on ^9Be elastic scattering was found to conform reasonably well to optical model predictions. The reaction cross sections were shown to be very small (2 to 200 $\mu\text{b}/\text{sr}$) at the energies used and have very little structure. The cross sections for an individual reaction product demonstrated an increase both with energy and excitation energy. Had better statistics been available, perhaps more structure would have been evident in these distributions.

The authors are indebted to Drs. R. R. Carlson and G. L. Payne for useful discussions during the course of this experiment.

References

- 1) E. Norbeck and R. C. York, Nucl. Instr. 118 (1974) 327
- 2) P. L. Von Behren, E. Norbeck and G. L. Payne, Phys. Rev. C10 (1974) 550
- 3) L. D. Landau and E. M. Lifshitz, Quantum mechanics (Addison-Wesley, Reading, Mass., 1958) p. 425
- 4) W. R. Smith, University of Southern California Report 136-119 (unpublished) (1967)
- 5) J. E. Poling, E. Norbeck and R. R. Carlson, Phys. Rev. C13 (1976) 648